Hindawi
Mathematical Problems in Engineering
Volume 2018, Article ID 1095842, 11 pages
https://doi.org/10.1155/2018/1095842

Research Article

Full-Scale Reconstruction for Transmission Line Galloping Curves Based on Attitudes Sensors

Decheng Wu,[1] Shizhong Yang,[1,2] Lu Tao,[1] Hailin Cao ,[1,2] Xiaoheng Tan,[3] Li Jing,[1] and Wenjian Qin[4,5]

[1]*Center of Tracking, Telemetering & Command and Communication, Chongqing University, Chongqing, China*
[2]*State Key Laboratory of Power Transmission Equipment & System Security and New Technology, Chongqing University, Chongqing, China*
[3]*College of Communication Engineering, Chongqing University, Chongqing, China*
[4]*Shenzhen Institutes of Advanced Technology, Chinese Academy of Sciences, Shenzhen, China*
[5]*Shenzhen College of Advanced Technology, University of Chinese Academy of Sciences, Shenzhen, China*

Correspondence should be addressed to Hailin Cao; hailincao@cqu.edu.cn

Received 27 March 2018; Accepted 4 June 2018; Published 27 June 2018

Academic Editor: Alessandro Lo Schiavo

Caused by strong winds or nonuniform icing, conductor galloping is one of the major hazards that should be monitored in a timely fashion. In this paper, we proposed a new full-scale reconstruction method for transmission line curves based on the attitude sensors that uses only the tangential information and arc-length constraint. Meanwhile, a comparatively low-complexity algorithm is presented: (1) quaternion rotation to generate the tangent vectors; (2) a modified B-spline global interpolation to evaluate the curvature information; and (3) a linear mapping method to correct reconstruction curves. Moreover, sensors placement method is put forward according to the galloping features. Finally, both simulation and experimental results demonstrate that the proposed method can accurately reconstruct the galloping curves in a relatively short time, which fulfills the requirement of the real-time galloping monitoring system.

1. Introduction

The overhead transmission line is the primary approach for long-distance electrical energy transmission, which is always challenged by the harsh environmental conditions. Caused by strong winds or nonuniform icing, conductor galloping is a kind of self-excited vibration with low frequency (0Hz-3Hz) and high amplitude (a few meters to tens of meters), and that can cause various types of damage, such as conductor fracture, tower collapse, and large-scale grid paralysis. Hence, galloping prevention is imperative [1–3].

Since the famous galloping vertical and torsional mechanism was proposed by Den Hartog [4] and Nigol [5], extensive studies have been performed on the galloping phenomenon. Recently, several researchers have theoretically investigated the galloping mechanism, and mathematical models have been presented to simulate the dynamical behavior of transmission [6–9]. Other authors have attempted to establish equations of motion to describe the observed three-dimensional galloping behavior on iced transmission lines [10, 11]. Moreover, Finite Element Method-based (FEM-based) approaches [12, 13] with various analytical tools, such as ABAQUS [14] and FLUENT [15], have been applied in numerical investigations on aerodynamic galloping problems. Furthermore, full-scale test transmission lines [1, 3] and wind tunnels [16] have been established to test the galloping behavior and antigalloping techniques, but some limitations remain. Although such studies have been performed in both theory and practice, there is no universal theory to explain the galloping mechanism.

Galloping data play an important role in the mechanism and effect analysis of dancing prevention. They can be crucial means to verify the antigalloping design theory and determine the galloping prevention plan and effect [17]. Unlike theoretical studies on the galloping mechanism, many authors have focused on the operation-state monitoring for

the transmission line using various techniques and sensor devices. The maximum galloping amplitudes [3, 18] and conductor sags [19] are the most common parameters to investigate dancing. Using the differential global positioning system (DGPS) to achieve the real measurement of the conductor position is probably the most direct method for obtaining conductor sag information, but it lacks full-scale galloping information [19]. Video- and image-processing [20] and photography methods [17, 21] have been explored to detect the spatial parameters of transmission lines. However, they are easily affected by rough weather conditions such as dense fog or heavy rain. Moreover, using video cameras for transmission line galloping requires many storages and transmission resources. A new fiber Bragg grating (FBG) sensor was applied to achieve the real-time horizontal tension monitoring of a transmission line, and the galloping amplitude could be calculated from the relationship between the galloping amplitude and the horizontal tension [22]. A new noncontact monitoring technology of operation-sate monitoring for high-voltage transmission lines is presented and uses the correlation between the magnetic-field variation and the electrical and spatial parameters of the transmission line [23]. A sensor module for galloping monitoring was designed using the inertial measurement unit (IMU) and wireless communication, and it can measure the conductor displacements along three directions [24]. Nevertheless, most existing studies are limited to a single point of the single conductor, which is difficult to cover the full-scale transmission line intuitively.

Unlike the aforementioned methods, this paper focuses on the full-scale reconstruction of the transmission lines. We aim to reconstruct the galloping curves via tangential information with a length constraint using few attitude sensors, which do not need to know the spatial position of the conductor obtained using DGPS technology. There have been a few studies of shape sensing using attitude sensors, such as Morphosense (a flexible ribbon-like device) [25] and Human wearing vest (with integrated shape sensing sensor array) [26]. The author in [25] proposed a spatial interpolation with a Pythagorean-hodograph, which has better reconstruction performance than does the natural cubic spline method. However, this method requires extensive iterative computations, which is not suitable for a real-time galloping monitoring system. Reference [26] presented a fast computation algorithm for the global shape reconstruction. Since the reconstruction precision is notably limited, many sensors must be used to ensure the reconstruction performance. Similarly, this method is not suitable for transmission line monitoring system because of the requirement of high sensor density. In this paper, we reconstruct the galloping curves by using a few attitude sensors, and a low-complexity algorithm is designed for the curve reconstruction. Using an attitude sensor that contains 9 axes (3 axes of gyroscope, accelerometer, and magnetometer), we can obtain conductor tangential information. Here, we only know the dip angle and length information of the conductor from a few attitude sensors. It should be noted that this problem is not a simple spline interpolation problem because the absolute spatial locations of the sensor nodes are not known. Because all directions of the 3-dimensional unit tangent vectors form a sphere, which is known as the Gaussian sphere, a simple and reasonable assumption of the tangent vectors between consecutive sensors is the geodesic of the given sensors. We use the quaternion rotation operation to fulfill the tangent information between the sensors. The "angular velocity" of the rotation, i.e., the curvature of the transmission line curves, remains unknown. With the curvilinear distances and rotation angles between successive sensors, a modified B-spline global interpolation is introduced to evaluate the curvature of the transmission line. Then, when the global tangent information and length parameter are combined, the desired galloping curves are reconstructed by integral operation. Moreover, due to the integral accumulated error effect, the reconstruction curve may cause a bias to the actual one, and this effect increases with the increase in integral length. According to the prior position information of the transmission tower, a linear mapping method is applied for curve correction, which can fix the reconstruction better to fit the real one. The reconstructed galloping curves can offer a visual method to monitor the galloping and extract galloping parameters such as amplitude, frequency, and waveform.

We believe, to the best of our knowledge, that this paper is the first study to attempt to examine the full reconstruction of galloping curves from a set of tangential information with the arc-length constraints.

2. Transmission Line Galloping Monitoring System

The transmission line galloping monitoring system [27] is shown in Figure 1. The attitude sensors are deployed on the transmission line to monitor the angle information at a predefined rate periodically. The sensor nodes disseminate the acquired data in real time or timed to the tower monitoring extension using the wireless network. The transmission line galloping includes the horizontal swing, vertical vibration, and axial torsion, which correspond to displacement in three orthogonal directions (x-, y-, and z-axes). Each attitude sensor can provide three-angle information, i.e., the pitch, roll, and yaw of the current position, and each has a separate controller and a power supply. Also, the number of sensors depends on the span of the transmission line and measurement accuracy, which should meet the requirement that there is not more than one galloping wave between the adjacent sensors. The tower monitoring extension gathers the uploaded information from each node, analyzes the data, and makes the appropriate data processing. The valid output data are sent to the monitoring center via the remote communication technology (Internet). Then, the full-scale transmission line curve is reconstructed in the monitoring center, and the galloping parameters (amplitude, frequency, and waveform) can be analyzed from the reconstructed data.

Obviously, the design of a sensor module should consider various factors: (1) electrical properties, e.g., visual corona and radio interference, resistance of short-circuit current rush, indirect lightning stroke, temperature rising property, and impulse stability; (2) electromagnetic compatibility, such

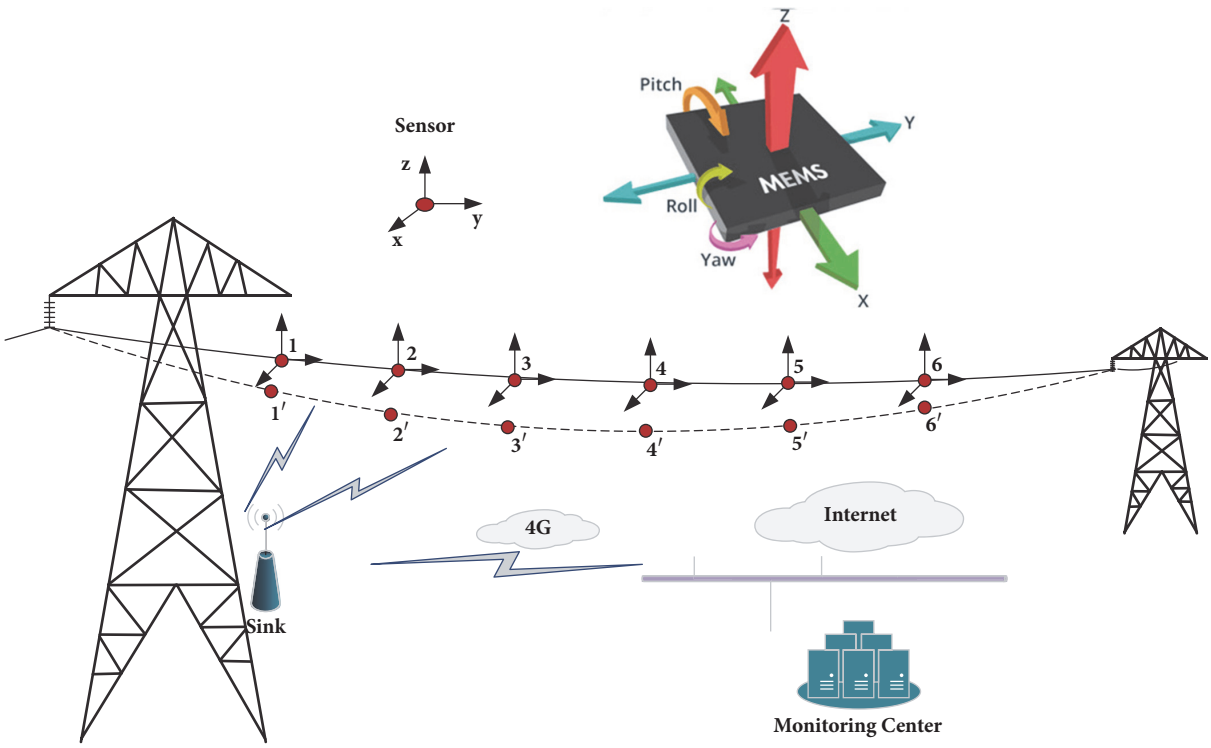

FIGURE 1: Diagram of the transmission line galloping monitoring system with six sensors.

as electrostatic discharge, radiated susceptibility, pulse magnetic field immunity, and power frequency magnetic field immunity; (3) climatic protection, such as high-temperature performance, low-temperature performance, and hydrothermal properties; (4) mechanical characteristics, including vibration-resistance performance antifatigue property [27]. Recently, many monitoring sensors have been designed and put into actual test for transmission line galloping monitoring. The authors in [28] have developed a cable inspection robot to acquire light detection and ranging (LiDAR) data. Also, the authors in [24] have designed a wireless sensor module with smooth spherical structure shell, and it contains an inertial measurement unit and wireless communication components. Since this is an original study; this paper focuses on the reconstruction method via tangential information with a length constraint using few attitude sensors.

We formulate the problem to design a space curve C(s):

$$\mathbf{C}(s) = \mathrm{P}_0 + \int_0^s \mathbf{t}(s)\, ds, \quad s \in [0, Ls] \tag{1}$$

where P_0 is the initial point (location of transmission tower), Ls is the length of the transmission line, and $\mathbf{t}(s)$ is the tangent vector with the arc-length parameter s. Obviously, we must reasonably calculate $\mathbf{t}(s)$ with the dip angle information from the attitude sensors.

3. Galloping Curve Reconstruction Method

The curve reconstruction is not merely a classical interpolation problem because we do not know the position of the sensor nodes. Moreover, we cannot independently address the dip information in each dimension because the spatial tangent vector is an entity whose norm is 1. Fortunately, because all three-dimensional tangent vectors lie on the unit sphere [29, 30], we can always find a curve on the sphere to denote the tangent vectors between the arc joining sensor nodes. In this paper, we interpolate the tangent vectors using the quaternion rotation.

3.1. Tangential Information with Arc-Length Constraint. Historically, quaternions were conceived by Hamilton as extensions to complex numbers. A quaternion q is defined by

$$q = w + x\mathbf{i} + y\mathbf{j} + z\mathbf{k} = [(x, y, z), \mathrm{w}] = [\mathbf{v}, w] \tag{2}$$

where $\mathbf{v} = (x, y, \mathrm{z}) \in \mathbb{R}^3$, $\mathrm{w} \in \mathbb{R}$, and $\mathbf{i}$, $\mathbf{j}$, and $\mathbf{k}$ are different imaginary units with $\mathbf{i}^2 = \mathbf{j}^2 = \mathbf{k}^2 = \mathbf{ijk} = -1$. More detailed properties of quaternions can be found in [31].

Given a unit quaternion $q \in \mathbb{S}^3$, i.e., $N(q) = qq^* = 1$, particularly if $q = \cos\theta + \mathbf{v}_0 \sin\theta \in \mathbb{S}^3$ for an angle θ and an arbitrary vector $\mathbf{t} = [(x, y, \mathrm{z}), 0]$, the 3D rotation operation is defined as

$$Q(\mathbf{t}) = q\mathbf{t}q^{-1} \tag{3}$$

where $Q(\mathbf{t})$ denotes the rotation by 2θ around the axis $\mathbf{v}_0$.

For example, let $\mathbf{v}_0$ be a unit vector with inclination (or elevation) angle α and azimuth angle β. Then, $q = [(\sin\alpha\cos\beta\sin\theta, \sin\alpha\sin\beta\sin\theta, \cos\alpha\sin\theta), \cos\theta]$, and $\mathbf{t}_2$ is the vector after the rotation operation; i.e., $\mathbf{t}_2 = Q(\mathbf{t}_0)$, as shown in Figure 2. Essentially, the rotation $Q(\mathbf{t}) = q\mathbf{t}q^{-1}$ is

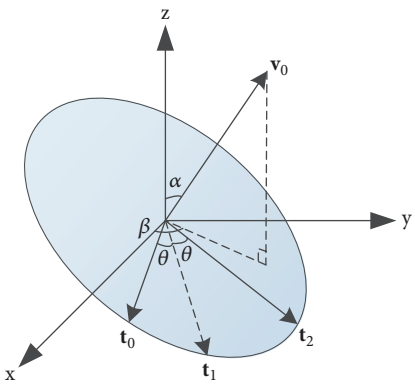

FIGURE 2: Geometry of rotation for a given axis $\mathbf{v}_0$ and vector $\mathbf{t}_0$.

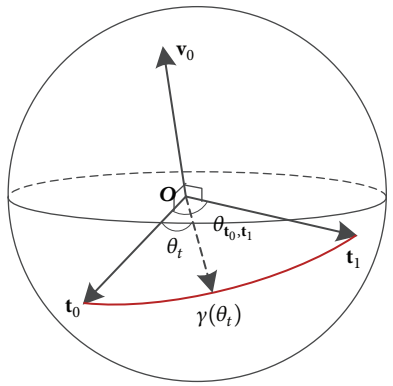

FIGURE 3: Geodesic curve for given tangent vectors $\mathbf{t}_0$ and $\mathbf{t}_1$.

divided into two steps. First, $\mathbf{t}_1$ is obtained from a θ rotation around the axis $\mathbf{v}_0$ from $\mathbf{t}_0$; i.e., $\mathbf{t}_1 = q\mathbf{t}_0$. Second, $\mathbf{t}_2$ is obtained from a θ rotation around the axis $\mathbf{v}_0$ from $\mathbf{t}_1$; i.e., $\mathbf{t}_2 = \mathbf{t}_1 q^{-1}$.

Now, we return to the problem of $\mathbf{t}(s)$ interpolation. By exploring the attitude sensor, we can obtain the 3-dimensional angle information, which can be converted into tangential information. The tangent vectors are unit vectors that lie on the Gaussian sphere.

A simple and possible answer is that these unknown tangential coefficients lie on the great arc between points $\mathbf{t}_0$ and $\mathbf{t}_1$, as shown in Figure 3. This arc is named the geodesic curve and is in $\mathbb{S}^2$ instead of $\mathbb{S}^3$, which is given by

$$\gamma(\theta_t) = q(\theta_t)\,\mathbf{t}_0, \quad \theta_t \in [0, \theta_{0,1}] \tag{4}$$

$$q(\theta_t) = [\mathbf{v}_0 \sin\theta_t, \cos\theta_t] = \exp(\mathbf{v}_0\theta_t) \tag{5}$$

where $\theta_{t_0,t_1} = \cos^{-1}(\|\mathbf{t}_0 \bullet \mathbf{t}_1\|) \in (0^\circ, 180^\circ]$ is the angle between vectors $\mathbf{t}_0$ and $\mathbf{t}_1$. $\mathbf{v}_0 = (\mathbf{t}_0 \times \mathbf{t}_1)/\|\mathbf{t}_0 \times \mathbf{t}_1\|$ is a unit vector in the direction of the cross-product of $\mathbf{t}_0$ and $\mathbf{t}_1$.

According to the arc-length constraint, θ_t is a variable that is associated with the arc-length parameters s, i.e., $\theta_t(\mathrm{s})$, and it satisfies $\theta_t(0) = 0$ and $\theta_t(l_{t_0,t_1}) = \theta_{t_0,t_1}$, where l_{t_0,t_1} is the arc-length between contiguous sensor nodes. Now, we obtain t(s) between the first two sensor nodes as follows:

$$\mathbf{t}(s) = \gamma(\theta_t(\mathrm{s})) = q(\theta_t(\mathrm{s}))\,\mathbf{t}_0, \quad \mathrm{s} \in \left[0, l_{t_0,t_1}\right]. \tag{6}$$

3.2. Curvature Information Using B-Spline Interpolation. From (6), we obtain the curvature $\kappa(s)$:

$$\begin{aligned}\kappa(s) &= \left|\frac{d\mathbf{t}(s)}{ds}\right| = \left|q'(\theta_t(\mathrm{s}))\,\mathbf{t}_0\theta_t'(\mathrm{s})\right| \\ &= \left|q'(\theta_t(\mathrm{s}))\,\mathbf{t}_0\right| \cdot \left|\theta_t'(\mathrm{s})\right| = \left|\theta_t'(\mathrm{s})\right|, \\ &\qquad \mathrm{s} \in [0, l_{0,1}].\end{aligned} \tag{7}$$

Since $q'(\theta_t(\mathrm{s}))$ and $\mathbf{t}_0$ are unit quaternions, the multiplication $|q'(\theta_t(\mathrm{s}))\mathbf{t}_0| = 1$. Therefore, the curvature $\kappa(s)$ depends on $\theta_t'(\mathrm{s})$ or $\theta_t(\mathrm{s})$.

A simple example is $\theta_t(\mathrm{s}) = (\theta_{0,1}/l_{0,1})s$, $s \in [0, l_{0,1}]$. Apparently, $\kappa(s) = \theta_t'(\mathrm{s}) = \theta_{0,1}/l_{0,1}$ is a constant, and the resulting curve (1) is a circular arc, which is not suitable for the situation of the transmission galloping curve.

Now, the calculation of $\mathbf{t}(s)$ is transformed into the problem of evaluating $\theta_t(\mathrm{s})$. Since the transmission line is an entire conductor, there is an internal connection between successive sensor nodes. Thus, a modified form of B-spline interpolation is introduced to estimate the curvature information.

When $n+1$ attitude sensors are placed, attitude sensors are placed, the length of the transmission line in each interval $l_{i,i+1}$ is determinate. Meanwhile, the angles $\theta_{i,i+1}$ between successive sensors can be calculated using $\theta_{i,i+1} = \cos^{-1}(\|\mathbf{t}_i \bullet \mathbf{t}_{i+1}\|)$, $0 \le i \le n$. We cumulatively reform the rotation angles and arc-lengths as follows:

$$s_0 = 0,\ s_1 = l_{0,1},\ \cdots,\ s_n = \sum_{i=0}^{n-1} l_{i,i+1} \tag{8}$$

$$\theta_0 = 0,\ \theta_1 = \theta_{0,1},\ \cdots,\ \theta_n = \sum_{i=0}^{n-1} \theta_{i,i+1}. \tag{9}$$

We obtain the data points $\boldsymbol{\theta} = [\theta_0, \theta_1, \cdots, \theta_n]$ with the corresponding parameter $\mathbf{s} = [s_0, s_1, \cdots, s_n]$, and the global curve of $\theta(\mathrm{s})$ is obtained by the classical B-spline interpolation, as shown in Figure 4.

Then, we calculate each segment of the rotation angle information as

$$\theta_{i,i+1}(s) = \theta(s) - \theta_i, \quad for\ 0 \le i \le n-1. \tag{10}$$

Then, we revise (6) in the global frame, and the tangent curve $\mathbf{t}(s)$ is reformulated by

$$\mathbf{t}(s) = \left(\prod_{i=0}^{n} \exp(\mathbf{v}_i\theta_t(\mathrm{s}))\right)\mathbf{t}_0, \quad s \in [0, s_n] \tag{11}$$

$$\mathbf{v}_i = \frac{(\mathbf{t}_i \times \mathbf{t}_{i+1})}{\|\mathbf{t}_i \times \mathbf{t}_{i+1}\|}. \tag{12}$$

By combining (1) and (11) with (12), the desired transmission line galloping curve can be reconstructed.

3.3. Reconstruction Curve Correction. In the actual situation, the results will be affected by the measurements. The errors

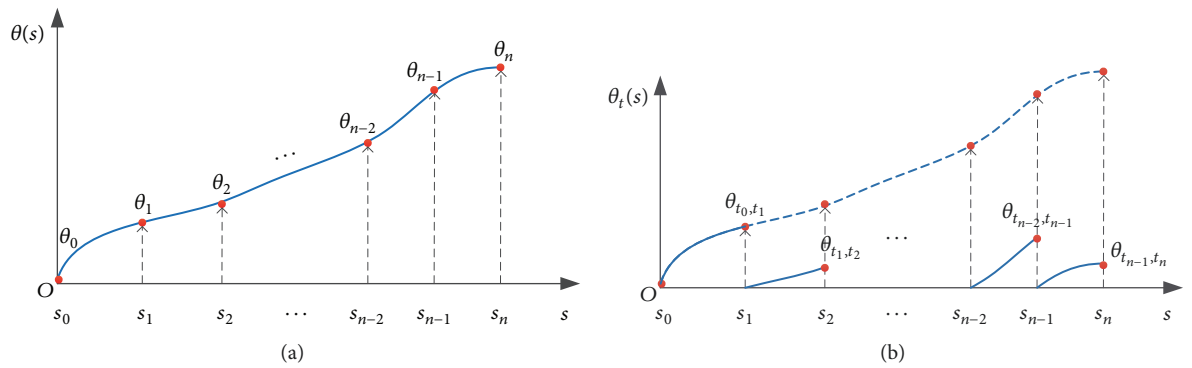

FIGURE 4: Diagram of the B-spline global interpolation curve (a) θ(s); (b) θ_t(s).

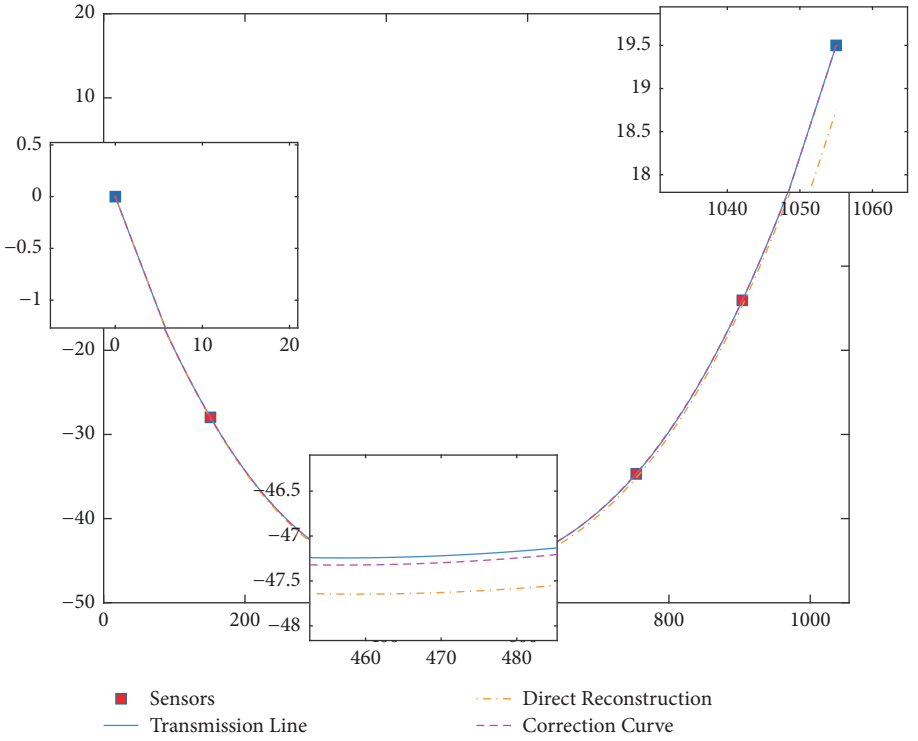

FIGURE 5: Reconstructions of the transmission lines: galloping curves with $Ns = 8$ sensors (red square), direct reconstruction curve (yellow dotted line), and correction curve (pink dash line).

from the sensors will have a direct impact on the shape of the reconstruction curves. Moreover, the error increases at the end of the reconstruction curve because of the integral accumulated error. Because the location of the two transmission towers is determined, we correct the curve using the linear mapping

$$x_c = \frac{\mathbf{p}_l(x) - \widehat{\mathbf{p}}_l(x)}{l} \times x + x$$
$$y_c = \frac{\mathbf{p}_l(y) - \widehat{\mathbf{p}}_l(y)}{l} \times x + y \quad (13)$$
$$z_c = \frac{\mathbf{p}_l(z) - \widehat{\mathbf{p}}_l(z)}{l} \times x + z$$

where $\mathbf{p}_l$ and $\widehat{\mathbf{p}}_l$ denote the transmission tower positions in reality and reconstruction, respectively; l is the span of the transmission tower; x is the span distance to the first transmission tower, $0 \le x \le l$; and (x, y, z) and (x_c, y_c, z_c) are the three-dimensional coordinates of the reconstruction and correction, respectively. The endpoint of the reconstruction curve clearly matches the transmission tower after the correction. In addition, if the reconstruction of the suspension point is far from the real position, this situation is regarded as transmission line fault, which will be explained in the next section. The reconstruction curve after correction is shown in Figure 5.

4. Sensors Placement and Galloping Alert

Not only the number of attitude sensors but also the placement position will affect the reconstruction performance of

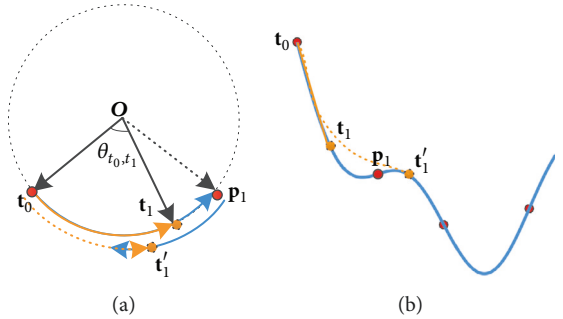

FIGURE 6: Illustration of the sensors installment. (a) The two-dimensional tangent vectors and (b) corresponding reconstruction curves.

galloping curves. To capture the galloping waves with the least number of sensors, the placement of the sensors should meet two conditions. (1) Ensure the angle variation between the two adjacent sensors is less than 180 degrees and (2) ensure this variation is monotonic.

Easy to illustrate, we take the two-dimensional curve as an example (three-dimensional case is likewise). The tangent vectors are unit vectors that formed a unit circle, as shown in Figure 6(a). The variation of the tangent vector can be interrupted as the rotation on the circle. In order to capture every waveform, the variation angle $\theta_{i,i+1}$ is not more than a half circle; i.e., $\theta_{i,i+1} \leq 180^\circ$, which is calculated as

$$\theta_{i,i+1} = \cos^{-1}\left(\left\|\mathbf{t}_i \bullet \mathbf{t}_{i+1}\right\|\right) \in \left(0^\circ, 180^\circ\right]. \quad (14)$$

Meanwhile, the variation should be monotonic; otherwise, partial curvature information will be lost. As shown in Figure 6(b), if the sensor node is installed at the position $\mathbf{t}'_1$ instead of $\mathbf{t}_1$, then curvature information from $\mathbf{t}_1$ to $\mathbf{t}'_1$ is missing. Meanwhile, we lost a galloping waveform between adjacent sensor nodes.

In summary, sensors should be ideally mounted on the inflection point of the curve. However, this condition is quite critical in the real application. We could not determine the position of the inflection point since transmission line galloping or change the position of sensors which had been placed on the transmission line. The other way to improve the reconstruction precision is to increase the number of sensors. For example, if we add another sensor node between $\mathbf{t}_1$ and $\mathbf{t}'_1$, then, we can get a better curve fitting to the real one.

The placement of sensors should match the galloping feature, i.e., the conduct sag [19] is easy ice-coating and galloping, and the place closer to the suspension ends is more fixed. Therefore, more sensors should be installed close to the conduct sag to capture more galloping information. In the study, a simple evenly installment method was proposed. We place the sensors evenly along the span direction, which can be mainly in line with the suspension characteristics of the transmission line. Moreover, as mentioned before, more sensors could get a better curve fitting to the real galloping curves. Figure 7 shows a case for sensor placements with different number of sensors. As we can see, $Ns = 6$ sensors mounted on the inflection point can achieve a fine performance. However, the performance gets worse when Ns increased to 8 with the even placement. But then Ns rises to 10 or more; the reconstruction can achieve acceptable accuracy.

With a proper number of sensors, the full-scale transmission line curve could be well reconstructed in the monitoring center. We can watch the reconstructed curves directly and can extract the galloping parameters (amplitude, frequency, and waveform) from the reconstructed data. It will be beneficial for the state monitoring and safety improvement of power delivery systems. For the case that the power transmission tower is slanted or collapsed, or the transmission line is fractured, as shown in Figure 8, the angle information will change accordingly, furthermore, the reconstruction curve will be greatly different (especially for the conductor sag and the suspension ends). These anomalous phenomena will be reflected directly in the reconstructed curves, so the workers can discover failure and repair the fault in the first time.

5. Simulation and Analysis

5.1. Simulation Setup. In this experiment, we used the single-degree-of-freedom (SDOF) model which only considers the vertical vibration to test the effectiveness of the method. The overhead transmission line curve with vertical vibration can be approximately formulated [3] as

$$y(x,t) = \frac{h}{l}x - \frac{\gamma x(l-x)}{2\sigma_0 \cos\beta} + A_0 \sin\left(\frac{n\pi}{l}x\right)\sin(\omega t) \quad (15)$$

where h (m) and l(m) are the height difference and span of the crossing tower, respectively. γ (MPa/m) is the specific load, which is defined as the load in the unit length and cross-sectional area. σ_0 (MPa) is the horizontal axial stress; $\beta = \arctan(h/l)$ is the angle of elevation difference. A_0 (m) denotes the galloping amplitude, n is the galloping loops, and ω(rad) is the galloping frequency. Using the transmission line parameters of the Great Span Project in Hubei province, China, the corresponding parameters are as follows: l=1055 m, h=19.5 m, $\gamma = 42.6\times10^{-3}$MPa/m, $\sigma_0 = 101.45$MPa, A_0=10 m, n=5, and ω=1.678 rad. In the simulation, we take the first five time slots of transmission line data as instances, as shown in Figure 9.

We set two evaluating indicators to assess the method performance. e_L indicates the length error between real

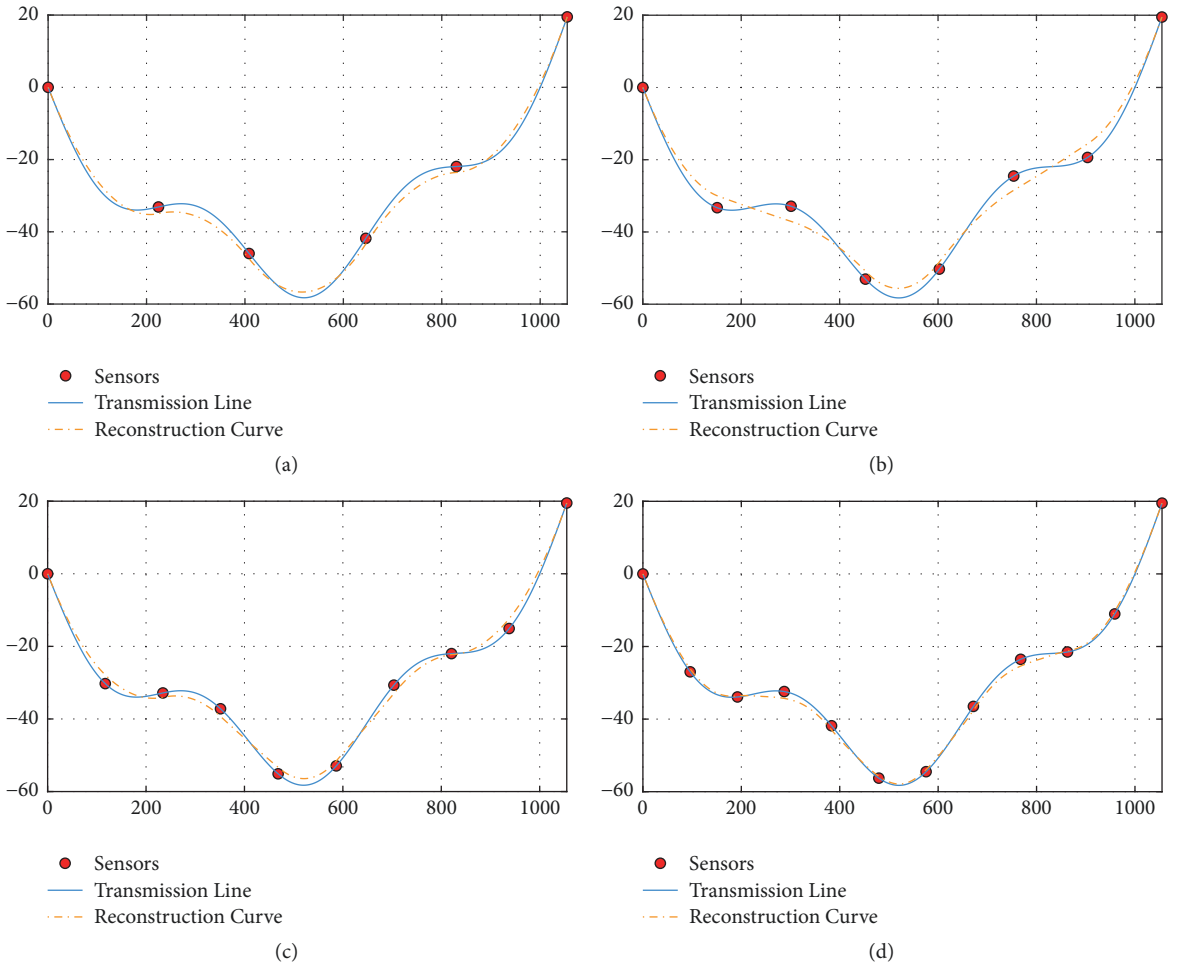

FIGURE 7: The reconstruction curves with different numbers of sensors. (a) $Ns = 6$ mounted on the inflection point. (b), (c), and (d) Evenly installed along the span with $Ns = 8$, $Ns = 10$, and $Ns = 12$, respectively.

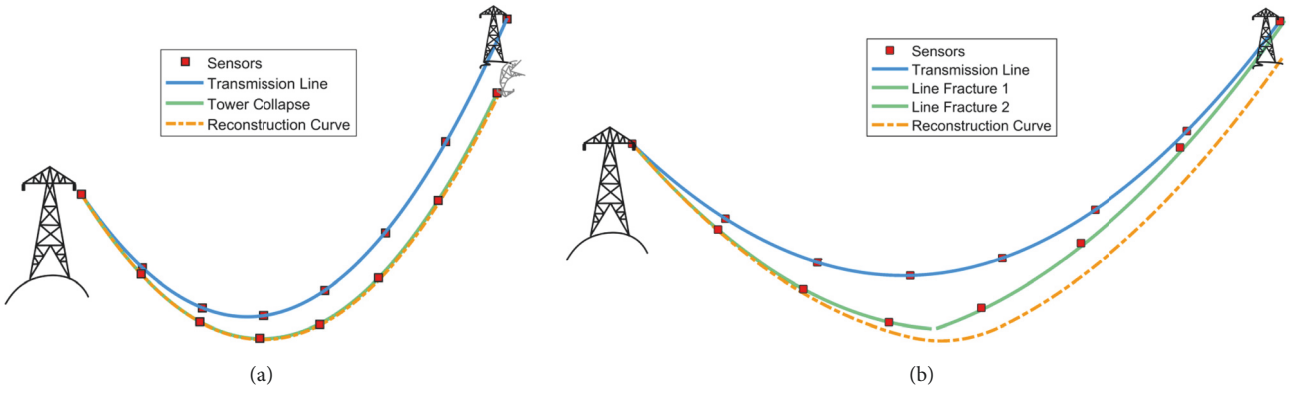

FIGURE 8: Illustration of the galloping alert for (a) tower collapse and (b) line fracture.

and reconstructed lengths of the transmission line and is expressed as

$$e_L = \frac{|Ls - Lr|}{Ls} \times 100\% \tag{16}$$

where Ls and Lr are the length of the transmission line and reconstruction length, respectively. e_P evaluates the reconstruction performance and is given by

$$e_P = \frac{1}{Ls}\frac{1}{Ns}\sum_{i=1}^{Ns} \left\|\mathbf{p}_i - \widehat{\mathbf{p}}_i\right\|_2^2 \times 100\% \tag{17}$$

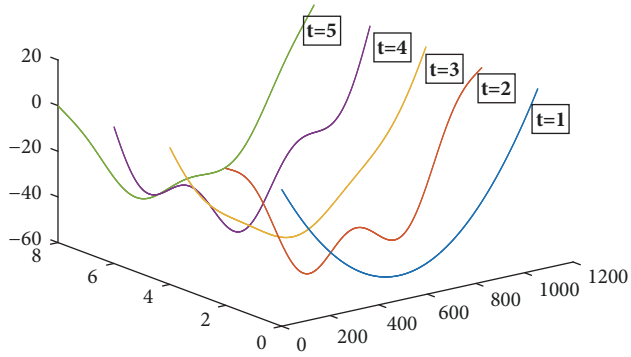

FIGURE 9: Illustration of SDOF galloping model in the first five time slots.

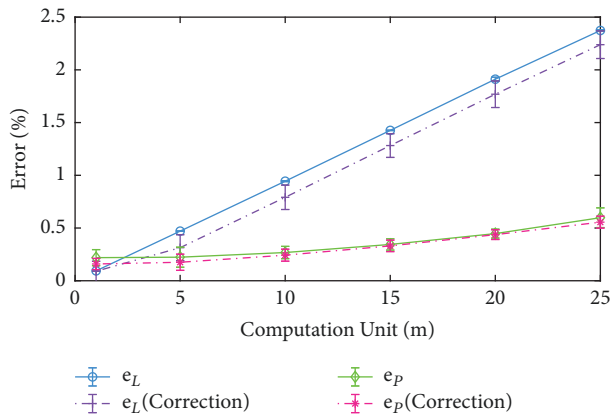

FIGURE 10: Reconstruction performance versus computation unit p_l.

where Ns is the number of sensors and $\mathbf{p}_i$ and $\widehat{\mathbf{p}}_i$ are the positions of the i-th attitude sensor in reality and reconstruction, respectively. To some extent, e_P represents the shape difference between the actual curves and the reconstructions.

5.2. Computation Unit p_l and Computational Complexity. The reconstruction performance is substantially dependent on the computation unit. In the simulation, Ns was fixed to 10 and the computation unit p_l was chosen as $p_l = [1, 5, 10, 15, 20, 25]$(m), and the reconstruction performance as shown in Figure 10. With p_l increasing, e_L rises sharply and e_P also shows a trend of slow growth. Therefore, p_l has a high impact on the length reconstruction. The bigger integrator unit leads to increased cumulative error. Meanwhile, the computation unit will directly decide the computational complexity. In this paper, all calculations were performed on a PC with a 3 GHz CPU (Intel Pentium G3220), and the corresponding average time consumption was $t = [0.903, 0.166, 0.086, 0.059, 0.046, 0.039]$(s). It is clear that, with the minor unit, the reconstruction will achieve higher precision but also higher computational complexity. It should be mentioned that, even with the minor unit $p_l = 1$ m, the average reconstruction time is less than one second, which meets the demand of the real-time application.

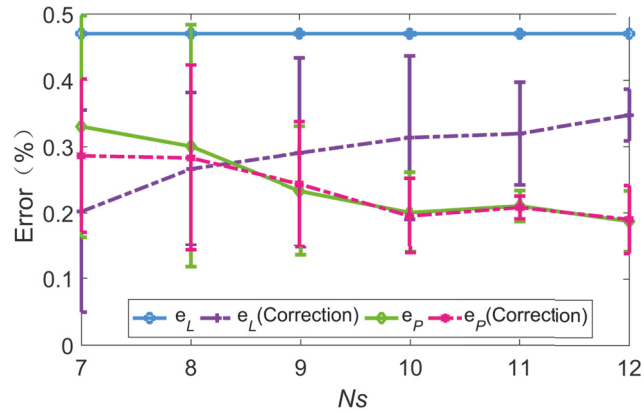

FIGURE 11: Reconstruction performance versus different numbers of sensors Ns.

5.3. Number of Sensors Ns. Figure 11 shows the reconstruction performance (error bar) versus different numbers of sensors. The computation unit p_l was fixed to 5 m and Ns was varied from 7 to 12 at the step of 1. It shows that Ns almost does not affect the length reconstruction e_L (as shown in blue line) and has a slow decline trend in the average position error e_P. This result is reasonable because more sensors lead to higher accuracy. When the sensors are twice than the galloping loops; i.e., $Ns = 10$, the average e_P has a sharp fall from 0.24% to 0.19%. Also, it can be observed that low bound of e_P with $Ns = 7$ is even lower than the one with $Ns = 11$. This situation is because that placement with $Ns = 7$ may be closed to the inflection point for some galloping time slots.

5.4. Curve Correction. As Figure 10 shows, when p_l is small (with $p_l = 1$m), the correction operation has limited effect for the reason that the reconstruction accuracy is relatively high. When p_l goes larger, correction operation can significantly reduce the length error e_L and also has slight improvement on the position error e_P. Moreover, as shown in Figure 11, it shows that correction operation can effectively adjust the length error induced by the computational unit $p_l = 5$m. Also it can successfully decrease e_P when sensors are not enough installed. When the sensors are more than twice of the galloping loops, the effect of correction operation is reduced since the algorithm achieves an acceptable reconstruction accuracy.

6. Experimental Test

Since this is an original work and limited by the experimental facility, a primary test platform in Figure 12(a) was built to verify the effectiveness of the proposed method. The span of the two hanging poles (simulated as transmission towers) is 9.2 m, and the length of the mooring rope (simulated as the transmission line) is 9.5 m. Eight sensor nodes (shown as red blocks) were evenly installed, in span direction, to capture the dip information (pitch angle and yaw angle). Since we ignore the twist of the test line, Roll angle information is not used in the experiment. The direction of the two hanging poles was

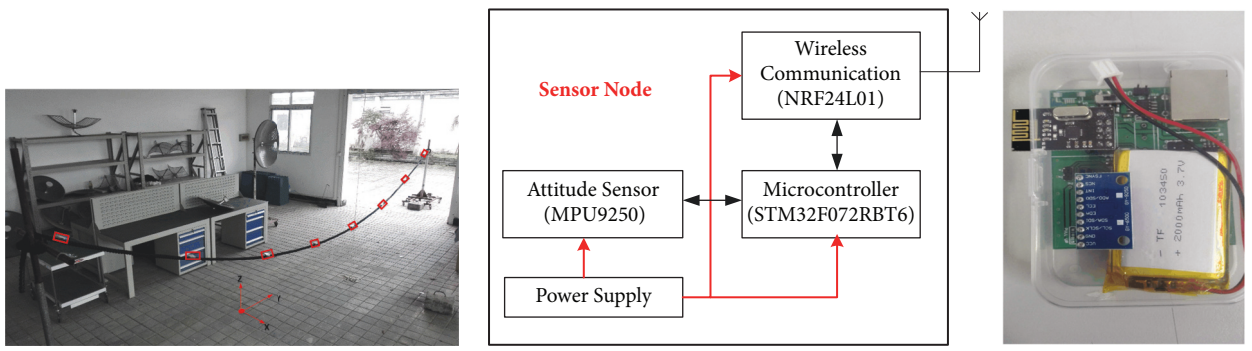

Figure 12: Test platform to simulate transmission line galloping: (a) experimental platform; (b) structure of the sensor node.

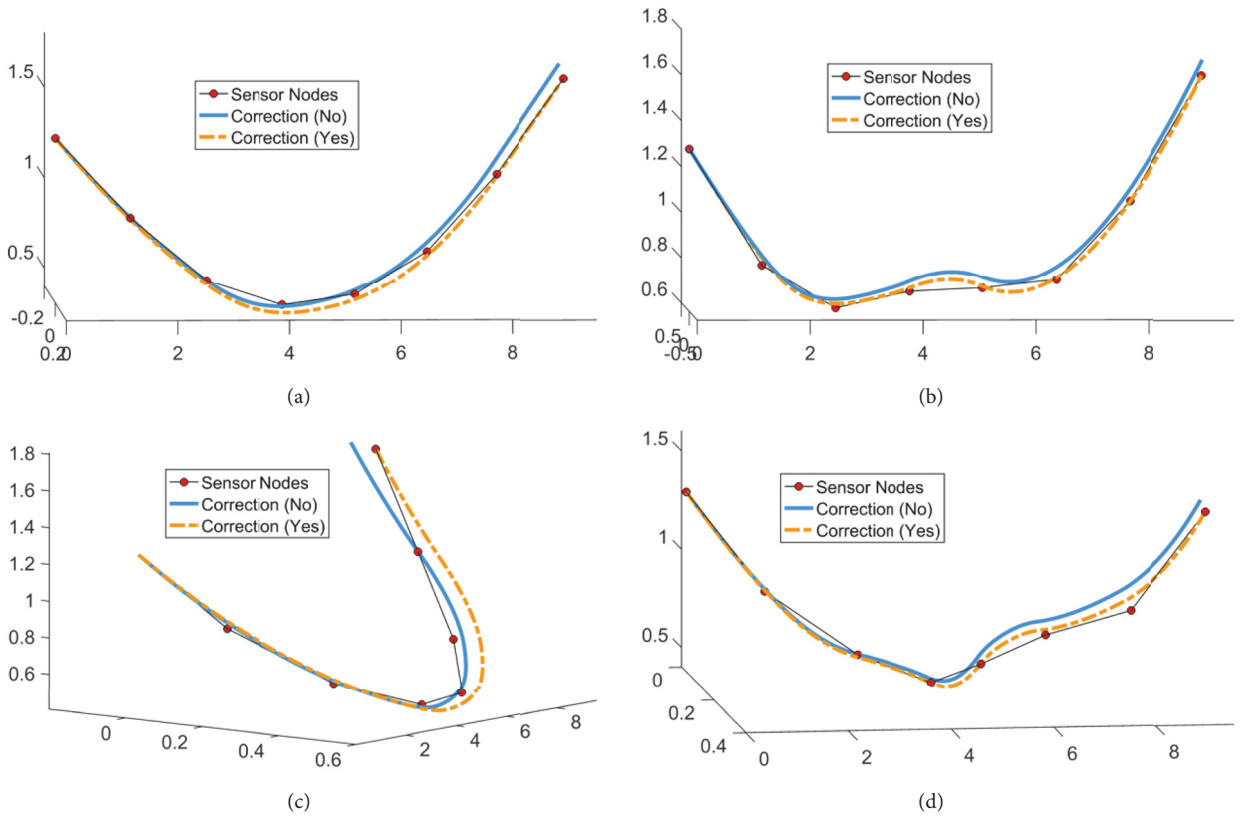

Figure 13: Experimental results of four different states. $Ns = 8$ sensors (red square) were explored on the test line. The reconstruction curves before and after the correction are denoted by the solid blue line and the dotted yellow line, respectively: (a) initial rest state; (b) vertical vibration; (c) horizontal swing; (d) tortuosity.

fixed to the y-axis, and the horizontal and vertical directions were set up as the x-axis and z-axis, respectively.

As shown in Figure 12(b), a sensor node was designed that consisted of an attitude sensor (MPU 9250), a wireless communication device (RF2401), microcontroller (STM32F072RBT6), and a power supply module. The attitude sensor was used to obtain the dip information. The microcontroller served as an interface between the attitude sensor and the wireless communication device and performed network-related tasks such as clock signal buffering and data retransmission.

Four states were set up to simulate the galloping curves: initial rest state, vertical vibration, horizontal swing, and tortuosity. In order to obtain the spatial position information of the sensor nodes, all the states were tested under static status. Meanwhile, two precision grids were set to p_l=0.01 m and p_l=0.1 m, and the reconstruction points $Ns = Ls/p_l$= 950 and 95 were used for reconstruction. The reconstruction performance was shown in Figure 13 (with p_l=0.01 m) and Table 1.

Because of the limitation of the experimental instrument, we observe that the real experimental result is worse than

Table 1: Reconstruction performance of four experimental states.

Time(s)	3.02 (p_l=0.01 m)				0.49 (p_l=0.1 m)			
Correction	No		Yes		No		Yes	
Error (%)	e_L	e_P	e_L	e_P	e_L	e_P	e_L	e_P
(a)	0.316	0.714	0.349	0.331	1.276	0.627	0.875	0.463
(b)	0.316	1.364	0.511	0.439	1.274	0.472	1.595	0.565
(c)	0.316	0.491	0.198	0.502	1.276	0.770	0.696	0.601
(d)	0.316	0.615	0.489	0.304	1.274	0.480	0.787	0.431
Mean	0.316	0.796	0.386	0.394	1.275	0.587	0.988	0.515

the simulated one. Nevertheless, the experimental results show that the reconstruction curves are reasonably consistent with the actual shape of the test lines. Comparing the direct reconstruction results and the corrected one, we observe that the correction operation increases the length error e_L slightly but decreases the position error e_P markedly. To some extent, e_P represents the shape difference between the original curves and the reconstructions. Thus, the reconstruction is closer to the original curve with smaller e_P, and the correction operation enhances the reconstruction curves by making them much closer to the actual one.

A comparison of the results with different precision grids clearly shows that p_l directly affects the reconstruction of the arc-length: $e_L = 0.316\%$ with $p_l = 0.01$m and $e_L = 1.275\%$ with $p_l = 0.1$m. However, p_l only slightly affects the reconstruction position error: $e_P = 0.394\%$ with $p_l = 0.01$m and $e_P = 0.515\%$ with $p_l = 0.1$m. The time consumption sharply decreases from 3.02 s to 0.49 s with a small increase in e_P. In other words, the proposed method costs less than 0.13s (with p_l=0.1 m) for one reconstruction, which is suitable for real-time monitoring of galloping systems.

7. Conclusions

This paper presents a new method for the full-scale reconstruction of transmission line galloping curves with few attitude sensors; the method uses only a set of tangential information with arc-length constraints instead of the spatial positions. With a small amount of dip information data from the attitude sensors, the galloping curves are reconstructed in the monitoring center, from which the transmission line galloping status during the monitoring time can be directly observed. Meanwhile, a low-complexity algorithm is introduced for the real-time reconstruction. We used the quaternion rotation to fulfill the tangent vectors between adjacent sensors, and the B-spline interpolation was applied to obtain the global curvature information. Moreover, a linear mapping was used to correct the reconstruction curves. In addition, we discussed the sensor installment and proposed a placement that sensors, with twice more than the galloping loops, were fixed evenly along the span direction. SDOF galloping model and an experimental platform were set up to verify the accuracy and applicability of the method. Both simulation and experimental results demonstrate that the proposed method can accurately reconstruct the galloping curves. Further, the average time cost of the proposed method is less than one second, which is suitable for real-time monitoring demands. This method can provide full-scale galloping trace information for power transmission line monitoring, which will be very helpful for the state monitoring and safety improvement of power delivery systems.

Data Availability

The data that support the findings of this study are available from the corresponding author upon reasonable request. (1) All data (except small part data in "experimental test") generated or analyzed during this study are within this article. The article has theoretical description about the data generation, and simulation data could be generated through the given equations in this article. (2) Data in "experimental test" are available from the corresponding author upon reasonable request. (3) Because of containing information that could compromise research participant privacy, source code is not publicly available. If researchers have any queries in the coding process, please do not hesitate to contact the authors.

Conflicts of Interest

The authors declare that they have no conflicts of interest.

Acknowledgments

This work was supported in part by the National Natural Science Foundation of China (nos. 51377179, 61301120, and 61571069), Guangdong province science and technology plan projects (Grant no. 2015B020233004), Natural Science Foundation of Chongqing (academician special) (no. cstc2014yykfys90001), and Project no. 106112017CDJQJ168817 supported by the Fundamental Research Funds for the Central Universities.

References

[1] P. van Dyke and A. Laneville, "Galloping of a single conductor covered with a D-section on a high-voltage overhead test line," *Journal of Wind Engineering & Industrial Aerodynamics*, vol. 96, no. 6-7, pp. 1141–1151, 2008.

[2] Z. Zhang, H. Li, G. Li, W. Wang, and L. Tian, "The numerical analysis of transmission tower-line system wind-induced

collapsed performance," *Mathematical Problems in Engineering*, vol. 2013, Article ID 413275, 11 pages, 2013.

[3] Y. K. Liu, Z. C. Fu, and X. H. Yang, "Galloping amplitude analysis and observation on full-scale test overhead transmission lines," *Power Energy Society General Meeting*, 2015.

[4] J. P. Denhartog, "Transmission line vibration due to sleet," *Electrical Engineering*, vol. 51, no. 6, pp. 413-413, 1932.

[5] O. Nigol and P. G. Buchan, "Conductor galloping and control based on torsional mechanism," in *Proceedings of the IEEE Transactions on Power Apparatus and Systems*, New York, America.

[6] N. Barbieri, O. H. de Souza Júnior, and R. Barbieri, "Dynamical analysis of transmission line cables. Part 1—Linear theory," *Mechanical Systems and Signal Processing*, vol. 18, no. 3, pp. 659–669, 2004.

[7] N. Barbieri, O. H. de Souza Júnior, and R. Barbieri, "Dynamical analysis of transmission line cables: part 2—damping estimation," *Mechanical Systems and Signal Processing*, vol. 18, no. 3, pp. 659–669, 2004.

[8] R. Barbieri, N. Barbieri, and O. H. de Souza Júnior, "Dynamical analysis of transmission line cables. Part 3-Nonlinear theory," *Mechanical Systems and Signal Processing*, vol. 22, no. 4, pp. 992–1007, 2008.

[9] B. Liu, K. Zhu, X. Li, and X. Zhan, "Hysteresis phenomenon in the galloping of the D-shape iced conductor," *Mathematical Problems in Engineering*, Art. ID 784239, 11 pages, 2013.

[10] Y. Wang, L. LÜ, and L. Huang, "Nonlinear vibration analysis for an airflow-excited translating string," *International Journal of Computational Methods*, vol. 9, no. 4, 1250051, 18 pages, 2012.

[11] W. Lou, L. Yang, M. F. Huang, and X. Yang, "Two-parameter bifurcation and stability analysis for nonlinear galloping of iced transmission lines," *Journal of Engineering Mechanics*, vol. 140, no. 11, 2014.

[12] D. Srivastava and D. Chandra, "Transmission line conductor galloping analysis using FEM," *International journal of applied engineering research*, vol. 11, no. 10, pp. 6972–6982, 2016.

[13] L. Zhou, B. Yan, L. Zhang, and S. Zhou, "Study on galloping behavior of iced eight bundle conductor transmission lines," *Journal of Sound and Vibration*, vol. 362, pp. 85–110, 2016.

[14] J. Hu, B. Yan, S. Zhou, and H. Zhang, "Numerical investigation on galloping of iced quad bundle conductors," *IEEE Transactions on Power Delivery*, vol. 27, no. 2, pp. 784–792, 2012.

[15] M. Cai, B. Yan, X. Lu, and L. Zhou, "Numerical Simulation of Aerodynamic Coefficients of Iced-Quad Bundle Conductors," *IEEE Transactions on Power Delivery*, vol. 30, no. 4, pp. 1669–1676, 2015.

[16] L. Xin-min, N. Xiao-chun, Z. Yong-kun, Y. Yi, and Y. Zhi-tao, "Wind Tunnel Tests on Aerodynamic Characteristics of Ice-Coated 4-Bundled Conductors," *Mathematical Problems in Engineering*, vol. 2017, pp. 1–11, 2017.

[17] W. Yang, Y. Shao, Z. Lv et al., "Study on monitoring for power transmission line galloping based on monocular vision method," in *Proceedings of the 2014 International Conference on Power System Technology, POWERCON 2014*, pp. 1571–1575, chn, October 2014.

[18] J. L. Lilien and D. G. Havard, "Galloping data base on single and bundle conductors prediction of maximum amplitudes," *IEEE Transactions on Power Delivery*, vol. 15, no. 2, pp. 670–674, 2000.

[19] S. M. Mahajan and U. M. Singareddy, "A real-time conductor sag measurement system using a differential GPS," *IEEE Transactions on Power Delivery*, vol. 27, no. 2, pp. 475–480, 2012.

[20] H. P. Ren and Z. F. Ma, "Transmission line galloping image monitoring system based on digital signal processor," in *Proceedings of SPIE - The International Society for Optical Engineering*, vol. 8009, pp. 1309–1311, 2011.

[21] H. Huang et al., "Transmission line icing measurement on photogrammetry method," in *Proceedings of the International Symposium on Multispectral Image Processing and Pattern Recognition*, 2015.

[22] Y. Chen, Z. Zhang, and X. Chen, "Novel monitoring method of power transmission line galloping based on fiber Bragg grating sensor," *Optical Engineering*, vol. 50, no. 11, pp. 114403–114406, 2011.

[23] X. Sun, Q. Huang, Y. Hou, L. Jiang, and P. W. T. Pong, "Noncontact operation-state monitoring technology based on magnetic-field sensing for overhead high-voltage transmission lines," *IEEE Transactions on Power Delivery*, vol. 28, no. 4, pp. 2145–2153, 2013.

[24] X. Huang, L. Zhao, and G. Chen, "Design of a wireless sensor module for monitoring conductor galloping of transmission lines," *Sensors*, vol. 16, no. 10, 2016.

[25] M. Huard, R. T. Farouki, N. Sprynski, and L. Biard, "C2 interpolation of spatial data subject to arc-length constraints using Pythagorean-hodograph quintic splines," *Graphical Models*, vol. 76, no. 1, pp. 30–42, 2014.

[26] A. Hermanis, R. Cacurs, and M. Greitans, "Acceleration and Magnetic Sensor Network for Shape Sensing," *IEEE Sensors Journal*, vol. 16, no. 5, pp. 1271–1280, 2016.

[27] Y. Hu, *Remote sensing inspection and monitoring technology for transmission lines*, China Power Press, 2012.

[28] X. Qin, G. Wu, X. Ye, L. Huang, and J. Lei, "A Novel Method to Reconstruct Overhead High-Voltage Power Lines Using Cable Inspection Robot LiDAR Data," *Remote Sensing*, vol. 9, no. 7, p. 753, 2017.

[29] K. T. Miura, "Unit quaternion integral curve: a new type of fair free-form curves," *Computer Aided Geometric Design*, vol. 17, no. 1, pp. 39–58, 2000.

[30] N. Sprynski, B. Lacolle, L. Biard, and D. David, "Curve and surface reconstruction via tangential information," in *Curve and surface design: Avignon 2006*, Mod. Methods Math., pp. 254–263, Nashboro Press, Brentwood, Calif, USA, 2007.

[31] D. H. Eberly and K. Shoemake, "Chapter 10 - Quaternions," in *Game PhysicsSan*, pp. 507–544, Morgan Kaufmann, San Francisco, 2004.